Electronic Research Archive

ERA, 31(12): 7544–7555.
DOI: 10.3934/era.2023380
Received: 27 September 2023
Revised: 21 November 2023
Accepted: 22 November 2023
Published: 28 November 2023

http://www.aimspress.com/journal/ERA

Research article

Contribution of a Ca^{2+}-activated K^{+} channel to neuronal bursting activities in the Chay model

Danqi Feng[1], Yu Chen[1] and Quanbao Ji[1,2,*]

[1] School of Mathematics and Physics, Guangxi Minzu University, Nanning 530006, China
[2] Center for Applied Mathematics of Guangxi, Guangxi Minzu University, Nanning 530006, China

* **Correspondence:** Email: jqb_2001@163.com.

Abstract: The central nervous system extensively expresses Ca^{2+}-stimulated K^{+} channels, which serve to use Ca^{2+} to control their opening and closing. In this study, we explore the numerical computation of Hopf bifurcation in the Chay model based on the equilibrium point's stability and the center manifold theorem to illustrate the emergence of complicated neuronal bursting induced by variation of the conductance of the Ca^{2+}-sensitive K^{+} channel. The results show that the formation and removal of various firing activities in this model are due to two subcritical Hopf bifurcations of equilibrium based on theoretical computation. Furthermore, the computational simulations are shown to support the validity of the conceptual approach. Consequently, the conclusion could be helpful to improve and deepen our understanding of the contribution of the Ca^{2+}-sensitive K^{+} channel.

Keywords: bifurcation; neuron; computation; burst

1. Introduction

It is known that the Chay model, comprising the mixed Na^{+}-Ca^{2+} channel current and K^{+} channel current, can be used to simulate and describe various neuronal firings of pancreatic β cells, sensory terminals and cold receptors [1–3]. Exploring the Chay model is prevalent to understand not only physical-mathematical associations but also physiological due to its simplicity and abundant dynamic behavior consisting of synchronization and oscillations set off by noise. Ca^{2+}-sensitive K^{+} channels are significant to the initiation of action potential, contributing substantially to physiological processes and its dysfunction leads to abnormal action potential propagation [4–6]. Bursting is crucial in the exchange of information between neurons, which is characterized by alternations between resting and repetitive firing states. The most significant messenger in cells is Ca^{2+}, which conveys vital information about nearly every action essential to the survival and proper operation of cells. The dynamic modulation of several elements is necessary for Ca^{2+} signaling, and the Na^{+}/Ca^{2+} exchanger (NCX) plays a role in maintaining its homeostasis by extracting Ca^{2+} from cells [7]. In both healthy and ischemic brains, astrocyte NCX activation may perform various roles. Studies are amassing that demonstrate the importance of one of the major glial ion transporters, NCX, in the regulation of astrocytic, microglial and oligodendrocytic functions. We can conjecture that alterations in NCX activity in distinct brain regions or astrocytic places may be linked to learning, memory and information processing functions in the brain [8]. It has become clear that neuronal firing patterns are usually associated with abundant dynamical behaviors since it is affected by intrinsic and extrinsic mediators, for instance, variation of ion path permeability, time delay and noise perturbation, as well as depolarizing current and so on [9–11]. Although nervous systems are quite different, neurons share many common features, such as action potential as carriers of information, ion channels and rich nonlinear phenomena.

Experimental and theoretical investigations indicate that action potentials generated by Na^{+}, Ca^{2+} and K^{+} currents are attributed to Ca^{2+}-activated K^{+} channels [12–14]. Due to the importance of electrical activities associated with Ca^{2+}-activated K^{+} channels, the dynamic mechanism underlying bursting in the Chay model should be investigated in detail. This model was studied extensively by Duan et al. [15–17], Xu et al. [18,19], Lu et al. [20,21] and Zhu et al. [22]. However, most studies are confined to numerical simulation of the Hopf bifurcation with variations in different bifurcation parameters [15–18]. Based on these previous works, the mechanisms and contributions involved in firing activities related to various ion channels are not well understood. Hence, we simulate the bursting dynamics associated with Ca^{2+}-activated K^{+} ion channels in combination with the use of the Chay model.

2. Stability and bifurcation analysis

We use the two-pool model by Chay [23] and develop upon it as a demonstration of stability and bifurcation analysis. This model is formed from three dynamic indexes: The membrane voltage (V), the concentration of Ca^{2+} within the cell (C) and the odds of triggering the voltage-sensitive K^{+} channel (n). The model comprises three equations:

$$\begin{cases} \dfrac{dV}{dt} = g_L^*(V_L - V) + g_{K,V}^* n^4 (V_K - V) + g_I^* m_\infty^3 h_\infty (V_I - V) + g_{K,C}^* \dfrac{C}{1+C}(V_K - V), \\ \dfrac{dC}{dt} = \rho\left[m_\infty^3 h_\infty (V_C - V) - k_C C \right], \\ \dfrac{dn}{dt} = \dfrac{n_\infty - n}{\tau_n}, \end{cases} \tag{1}$$

where

$$m_\infty = \frac{\alpha_m}{\alpha_m + \beta_m}, \qquad n_\infty = \frac{\alpha_n}{\alpha_n + \beta_n}, \qquad h_\infty = \frac{\alpha_h}{\alpha_h + \beta_h},$$

$$\alpha_m = \frac{0.1(25+V)}{1-e^{-0.1V-2.5}}, \qquad \beta_m = 4e^{\frac{-(V+50)}{18}}, \qquad \alpha_h = 0.07e^{-0.05V-2.5},$$

$$\beta_h = \frac{1}{1+(e^{-0.1V-2})}, \qquad \alpha_n = \frac{0.01(20+V)}{1-e^{-0.1V-2}}, \qquad \beta_n = 0.125e^{\frac{-(V+30)}{80}},$$

$$\tau_n = \frac{1}{\lambda_n(\alpha_n + \beta_n)}.$$

The details of each parameter can be found in [23]. Here, g^*_{kc} is designated as the bifurcation parameter. It represents the highest conductance of Ca^{2+}-sensitive K^+ channel. Let $x = V$, $y = C$, $z = n$, $r = g^*_{kc}$. In order to simplify the calculation process, system (1) is transformed into the subsequent expression:

$$\begin{cases} \dot{x} = \dfrac{126.0\mathrm{e}^{-0.05x-2.5}(x-100)(0.1x+2.5)^3}{\left(\mathrm{e}^{-0.1x-2.5}-1\right)^3\left(0.07\mathrm{e}^{-0.05x-2.5}+\dfrac{1}{\mathrm{e}^{-0.1x-2}+1}\right)\left(4\mathrm{e}^{-\frac{x}{18}-\frac{25}{9}}-\dfrac{0.1x+2.5}{\mathrm{e}^{-0.1x-2.5}-1}\right)^3}-1700z^4(x+75) \\ \qquad -\dfrac{ry(x+75)}{y+1}-7x-280, \\ \dot{y} = \dfrac{0.0189\mathrm{e}^{-0.05x-2.5}(x-100)(0.1x+2.5)^3}{\left(\mathrm{e}^{-0.1x-2.5}-1\right)^3\left(0.07\mathrm{e}^{-0.05x-2.5}+\dfrac{1}{\mathrm{e}^{-0.1x-2}+1}\right)\left(4\mathrm{e}^{-\frac{x}{18}-\frac{25}{9}}-\dfrac{0.1x+2.5}{\mathrm{e}^{-0.1x-2.5}-1}\right)^3}-0.0495y, \\ \dot{z} = -\left(28.75\mathrm{e}^{-\frac{x}{80}-\frac{3}{8}}-\dfrac{230(0.01x+0.2)}{\mathrm{e}^{-0.1x-2}-1}\right)\left(z+\dfrac{0.01x+0.2}{\left(\mathrm{e}^{-0.1x-2}-1\right)\left(0.125\mathrm{e}^{-\frac{x}{80}-\frac{3}{8}}-\dfrac{0.01x+0.2}{\mathrm{e}^{-0.1x-2}-1}\right)}\right). \end{cases} \tag{2}$$

The existence of equilibrium points can be determined by analyzing the differential equations of model. Suppose system (2) has three roots x_0, y_0, z_0. Let $x_1 = x - x_0$, $y_1 = y - y_0$, $z_1 = z - z_0$, we get the following representations:

$$\begin{cases} \dot{x}_1 = \dfrac{126.0\mathrm{e}^{-2.5-0.05(x_0+x_1)}\left((x_0+x_1)-100\right)\left(2.5+0.1(x_0+x_1)\right)^3}{\left(0.07\mathrm{e}^{-0.05(x_1+x_0)-2.5}+\dfrac{1}{\mathrm{e}^{-0.1(x_1+x_0)-2}+1}\right)\left(\mathrm{e}^{-0.1(x_1+x_0)-2.5}-1\right)^3\left(4\mathrm{e}^{-\frac{x_1+x_0}{18}-\frac{25}{9}}-\dfrac{0.1(x_1+x_0)+2.5}{\mathrm{e}^{-0.1(x_1+x_0)-2.5}-1}\right)^3} \\ \quad -1700(z_1+z_0)^4\left((x_1+x_0)+75\right)-\dfrac{(y_0+y_1)r\left((x_0+x_1)+75\right)}{y_1+y_0+1}-7(x_0+x_1)-280, \\ \dot{y}_1 = \dfrac{0.0189\mathrm{e}^{-0.05(x_1+x_0)-2.5}\left((x_1+x_0)-100\right)\left(0.1(x_1+x_0)+2.5\right)^3}{\left(0.07\mathrm{e}^{-0.05(x_1+x_0)-2.5}+\dfrac{1}{\mathrm{e}^{-0.1(x_1+x_0)-2}+1}\right)\left(\mathrm{e}^{-0.1(x_1+x_0)-2.5}-1\right)^3\left(4\mathrm{e}^{-\frac{x_1+x_0}{18}-\frac{25}{9}}-\dfrac{0.1(x_1+x_0)+2.5}{\mathrm{e}^{-0.1(x_1+x_0)-2.5}-1}\right)^3} \\ \quad -0.0495(y_1+y_0), \\ \dot{z}_1 = -\left(28.75\mathrm{e}^{-\frac{x_1+x_0}{80}-\frac{3}{8}}-\dfrac{230\left(0.01(x_1+x_0)+0.2\right)}{\mathrm{e}^{-(x_0+x_1)0.1-2}-1}\right) \\ \quad \left(z_1+z_0+\dfrac{0.2+(x_0+x_1)0.01}{\left(\mathrm{e}^{-0.1(x_1+x_0)-2}-1\right)\left(0.125\mathrm{e}^{-\frac{x_1+x_0}{80}-\frac{3}{8}}-\dfrac{0.01(x_1+x_0)+0.2}{\mathrm{e}^{-0.1(x_1+x_0)-2}-1}\right)}\right). \end{cases} \tag{3}$$

Equilibrium is (0, 0, 0) and system (3) has the same properties in system (2). It is clear that the Jacobian matrix $(a_{ij})_{3\times3}$ of system (3) and the characteristic equations satisfy: $\lambda^3 + Q_1\lambda^2 + Q_2\lambda + Q_1 = 0$, where $Q_3 = a_{31}a_{13}a_{22} + a_{12}a_{21}a_{33} + a_{32}a_{23}a_{11} - a_{11}a_{22}a_{33} - a_{12}a_{23}a_{31} - a_{13}a_{21}a_{32}$, $Q_2 = a_{11}a_{22} + a_{11}a_{33} + a_{22}a_{33} - a_{13}a_{31} - a_{12}a_{21} - a_{32}a_{23}$, $Q_1 = -(a_{11} + a_{22} + a_{33})$. Examine the Hurwitz matrix in the context of the coefficients Q_i ($i = 1, 2, 3$) of the characteristic polynomial:

$$H_1 = [Q_1],\ H_2 = \begin{pmatrix} Q_1 & 1 \\ Q_3 & Q_2 \end{pmatrix},\ H_3 = \begin{bmatrix} Q_1 & 1 & 0 \\ Q_3 & Q_2 & 1 \\ 0 & 0 & Q_3 \end{bmatrix}.$$

The eigenvalues are negative when the determinant values of Hurwitz matrix are bigger than zero:

$$\det(H_i) > 0,\ i = 1,2,3.$$

The robustness of system (3) is taken into account as varying the values of g^*_{kc} using the criteria of the Routh's array:

$$Q_1 > 0,\ Q_3 > 0,\ Q_1 Q_2 > Q_3.$$

It is easy to see that:

1) r < -41.647, system (3) contains a stable node;

2) r = -41.647, the system possesses a non-hyperbolic stationary state, which is O_1 = (-17.5904, 4.7463, 0.4334);

3) -41.647 < r < 27.25, the system includes a saddle point;

4) r = 27.25, the system contains a non-hyperbolic stationary state, which is O_2 = (24.7680, -0.8969, 0.6095);

5) r > 27.25, the system is stable.

The system (3) reaches equilibrium at (x_0, y_0, z_0) as $r = r_0$, $x_1 = x - x_0$, $y_1 = y - y_0$, $z_1 = z - z_0$, $r_1 = r - r_0$. Next, we introduce a new variable denoted as r_1 in the application of center manifold theorem with respect to the parameter g^*_{kc}. Let $dr_1/dt = 0$, we obtain:

$$\begin{cases} \dot{x}_1 = \dfrac{126.0\mathrm{e}^{-2.5-0.05(x_0+x_1)}\left((x_0+x_1)-100\right)\left(2.5+0.1(x_0+x_1)\right)^3}{\left(0.07\mathrm{e}^{-0.05(x_1+x_0)-2.5}+\dfrac{1}{\mathrm{e}^{-0.1(x_1+x_0)-2}+1}\right)\left(\mathrm{e}^{-0.1(x_1+x_0)-2.5}-1\right)^3\left(4\mathrm{e}^{-\frac{x_1+x_0}{18}-\frac{25}{9}}-\dfrac{0.1(x_1+x_0)+2.5}{\mathrm{e}^{-0.1(x_1+x_0)-2.5}-1}\right)^3} \\ \qquad -1700(z_0+z_1)^4\left((x_0+x_1)+75\right)-\dfrac{(y_0+y_1)\left((x_1+x_0)+75\right)(r_0+r_1)}{y_1+y_0+1}-7(x_1+x_0)-280, \\ \dot{y}_1 = \dfrac{0.0189\mathrm{e}^{-2.5-0.05(x_0+x_1)}\left((x_0+x_1)-100\right)\left(2.5+0.1(x_0+x_1)\right)^3}{\left(0.07\mathrm{e}^{-0.05(x_1+x_0)-2.5}+\dfrac{1}{\mathrm{e}^{-0.1(x_1+x_0)-2}+1}\right)\left(\mathrm{e}^{-0.1(x_1+x_0)-2.5}-1\right)^3\left(4\mathrm{e}^{-\frac{x_1+x_0}{18}-\frac{25}{9}}-\dfrac{0.1(x_1+x_0)+2.5}{\mathrm{e}^{-0.1(x_1+x_0)-2.5}-1}\right)^3} \\ \qquad -0.0495(y_1+y_0), \\ \dot{z}_1 = -\left(28.75\mathrm{e}^{-\frac{x_1+x_0}{80}-\frac{3}{8}}-\dfrac{230\left(0.01(x_1+x_0)+0.2\right)}{\mathrm{e}^{-2-0.1(x_0+x_1)}-1}\right) \\ \qquad \left(z_0+z_1+\dfrac{0.01(x_0+x_1)+0.2}{\left(\mathrm{e}^{-0.1(x_1+x_0)-2}-1\right)\left(0.125\mathrm{e}^{-\frac{x_1+x_0}{80}-\frac{3}{8}}-\dfrac{0.01(x_1+x_0)+0.2}{\mathrm{e}^{-0.1(x_1+x_0)-2}-1}\right)}\right), \\ \dot{r}_1 = 0. \end{cases} \tag{4}$$

As $r_1 = 0$, system (4) achieves equilibrium O (x_1, y_1, z_1, r_1) = (0, 0, 0, 0), which has the identical property in system (2). When r_0 = -41.647, we consider the characteristic values of balanced state O_1 = (0, 0, 0, 0) in system (4): ξ_1 = -0.0005, ξ_2 = 1.6305i, ξ_3 = -1.6305i, ξ_4 = 0.

Suppose

$$\begin{pmatrix} x_1 \\ y_1 \\ z_1 \\ r_1 \end{pmatrix} = U \begin{pmatrix} u \\ v \\ w \\ s \end{pmatrix}, \text{ where } U = \begin{pmatrix} 0.1263 & 1.0000 & 0 & -0.0829 \\ 0.9920 & 0 & 0 & 0.0022 \\ 0.0021 & 0.0001 & 0.0051 & -0.0014 \\ 0 & 0 & 0 & 0.9966 \end{pmatrix},$$

system (4) has the following form

$$\begin{pmatrix} \dot{u} \\ \dot{v} \\ \dot{w} \\ \dot{s} \end{pmatrix} = \begin{pmatrix} -0.0005 & 0 & 0 & 0 \\ 0 & 0 & -1.6305 & 0 \\ 0 & 1.6305 & 0 & 0 \\ 0 & 0 & 0 & 0 \end{pmatrix} \begin{pmatrix} u \\ v \\ w \\ s \end{pmatrix} + \begin{pmatrix} g_1 \\ g_2 \\ g_3 \\ g_4 \end{pmatrix}, \tag{5}$$

where

$$\begin{aligned}
g_1 &= 1.008064516 f_2 - 0.002225307983 f_4 + 0.0005u, \\
g_2 &= f_1 - 0.1273185484 f_2 + 0.08346387799 f_4 + 1.6305w, \\
g_3 &= -0.01960784314 f_1 - 0.4125889469 f_2 + 196.0784314 f_3 + 0.2747260781 f_4 - 1.6305v, \\
g_4 &= 0, \\
f_1 &= \frac{126.0\mathrm{e}^{-0.05g_{11}-2.5}(g_{11}-100)(0.1g_{11}+2.5)^3}{\left(0.07\mathrm{e}^{-0.05g_{11}-2.5}+\frac{1}{\mathrm{e}^{-0.1g_{11}-2}+1}\right)\left(\mathrm{e}^{-0.1g_{11}-2.5}-1\right)^3\left(4\mathrm{e}^{-\frac{g_{11}}{18}-\frac{25}{9}}-\frac{0.1g_{11}+2.5}{\mathrm{e}^{-0.1g_{11}-2.5}-1}\right)^3} \\
&\quad -1700g_{13}{}^4(g_{11}+75)-\frac{g_{14}g_{12}(g_{11}+75)}{g_{12}+1}-7g_{11}-280, \\
f_2 &= \frac{0.0189\mathrm{e}^{-0.05g_{11}-2.5}(g_{11}-100)(0.1g_{11}+2.5)^3}{\left(0.07\mathrm{e}^{-0.05g_{11}-2.5}+\frac{1}{\mathrm{e}^{-0.1g_{11}-2}+1}\right)\left(\mathrm{e}^{-0.1g_{11}-2.5}-1\right)^3\left(4\mathrm{e}^{-\frac{g_{11}}{18}-\frac{25}{9}}-\frac{0.1g_{11}+2.5}{\mathrm{e}^{-0.1g_{11}-2.5}-1}\right)^3} \\
&\quad -0.0495g_{12}, \\
f_3 &= -\left(28.75\mathrm{e}^{-\frac{g_{11}}{80}-\frac{3}{8}}-\frac{230(0.01g_{11}+0.2)}{\mathrm{e}^{-0.1g_{11}-2}-1}\right) \\
&\quad \left(g_{13}+\frac{0.01g_{11}+0.2}{\left(\mathrm{e}^{-0.1g_{11}-2}-1\right)\left(0.125\mathrm{e}^{-\frac{g_{11}}{80}-\frac{3}{8}}-\frac{0.01g_{11}+0.2}{\mathrm{e}^{-0.1g_{11}-2}-1}\right)}\right), \\
f_4 &= 0, \\
g_{11} &= x_1 + x_0 = 0.1263u - 0.0829s + 1.0v - 17.5904, \\
g_{12} &= y_1 + y_0 = 0.0022s + 0.992u + 4.7463, \\
g_{13} &= z_1 + z_0 = 0.0021u - 0.0014s + 0.0001v + 0.0051w + 0.4334, \\
g_{14} &= 0.9966s - 41.647.
\end{aligned}$$

Based on center manifold theorem, a center manifold exists. The specific form is as follows:

$$W_{loc}^{c}(O_1) = \{(u,v,w,s) \in R^4 \,|\, u = h^*(v,w,s),\ h^*(0,0,0) = 0,\ Dh^*(0,0,0) = 0\},$$

Assume $h(v, w, s) = av^2 + bw^2 + cs^2 + dvw + evs + fws + \ldots$, the center manifold is

$$N(h) = Dh \cdot \begin{bmatrix} \dot{v} \\ \dot{w} \\ \dot{s} \end{bmatrix} + 0.0005h - g_1 \equiv 0. \tag{6}$$

Here a = -0.0000036406, b = -0.000003093017389, c = 0.00008567728077, d = 0.00000180521, e = 0.00000016, f = -0.0000005491. If the system is limited by center manifold, the following conditions are satisfied:

$$\begin{pmatrix} \dot{v} \\ \dot{w} \end{pmatrix} = \begin{pmatrix} 0 & -1.6305 \\ 1.6305 & 0 \end{pmatrix} \begin{pmatrix} v \\ w \end{pmatrix} + \begin{pmatrix} f^1(v,w) \\ f^2(v,w) \end{pmatrix}, \tag{7}$$

where

$$\begin{aligned} f^1(v,w) &= 0.580313865s - 7.0v + 1.6305w - 0.0000001404922113sv + 0.0000004820211492sw \\ &\quad - 0.000001584700346vw + \cdots, \\ f^2(v,w) &= -0.01133350044s - 1.493245098v + 0.000000006016773356sv - 0.00000002064322272sw \\ &\quad + 0.00000006786698519vw + \cdots. \end{aligned}$$

Then, we have

$$\begin{aligned} a &= \frac{1}{16}[f^1_{vvv} + f^1_{vww} + f^2_{vvw} + f^2_{www}]\Big|_{(0,0)} + \frac{1}{16\times 0.0204}[f^1_{vw}(f^1_{vv} + f^1_{ww}) \\ &\quad - f^2_{vw}(f^2_{vv} + f^2_{ww}) - f^1_{vv}f^2_{vv} + f^1_{ww}f^2_{ww})]\Big|_{(v=0,w=0,s=0)} = 3.01538319 > 0, \\ d &= \left.\frac{d(\mathrm{Re}(\xi(s))}{ds}\right|_{(v=0,w=0,s=0)} = -0.00001623167121 < 0. \end{aligned} \tag{8}$$

According to previous numerical computations, we have:

Conclusion 1: At r_0 = -41.647, a supercritical Hopf bifurcation is obtained. When the value of r is less than r_0, the equilibrium O_1 turns to be stable. The equilibrium state loses stability as $r > r_0$ and a stable periodic solution appears, which causes the oscillation of system (2). As r_0 = 27.25, the characteristic values are $\xi_1 = 0.0036$, $\xi_2 = 3.8251i$, $\xi_3 = -3.8251i$ and $\xi_4 = 0$, respectively.

The simplified form based on the center manifold system (4) is depicted as

$$\begin{pmatrix} \dot{v} \\ \dot{w} \end{pmatrix} = \begin{pmatrix} 0 & -3.8251 \\ 3.8251 & 0 \end{pmatrix} \begin{pmatrix} v \\ w \end{pmatrix} + \begin{pmatrix} f^1(v,w) \\ f^2(v,w) \end{pmatrix}, \tag{9}$$

where

$$\begin{aligned} f^1(v,w) &= 0.62108\text{s} - 7.0v + 3.8251w - 0.000007826615347sv + 0.0000114824966\text{l}sw \\ &\quad - 0.0001076807683vw + \cdots, \\ f^2(v,w) &= -0.1979232s - 2.9851v + 0.000001122019432sv - 0.000001646124635sw \\ &\quad + 0.00001543705793vw + \cdots. \end{aligned}$$

The next conclusion can be obtained as $a = 0.32334838 > 0$ and $d = 0.01462214783 > 0$.

Conclusion 2: At r_0 = 27.25, the system exhibits a subcritical Hopf bifurcation transition. As r is less than r_0, the equilibrium O_2 is in an unstable state. As $r > r_0$, the equilibrium O_2 returns to be stable.

3. Numerical simulations

The generation processes of the parameter g^*_{kc} are presented so as to study the bifurcation phenomenon underlying various firing activities. Figures 1(a),(b) show the bifurcations that illustrate the stationary states of system (2) in the (V, g^*_{kc}) and (C, g^*_{kc}) planes, respectively. Each point of the solid line in the curve denotes equilibrium stability, and the dotted curve is an unsteady stationary state. Additionally, g^*_{kc} passes through two Hopf bifurcations labeled with HB^1 and HB^2, where $g^*_{kc}{}^1 = -41.647$ μM/s and $g^*_{kc}{}^2 = 27.25$ μM/s. As g^*_{kc} is increased, the balanced stationary initially loses its steady state at HB^1, only to regain the balanced state at HB^2.

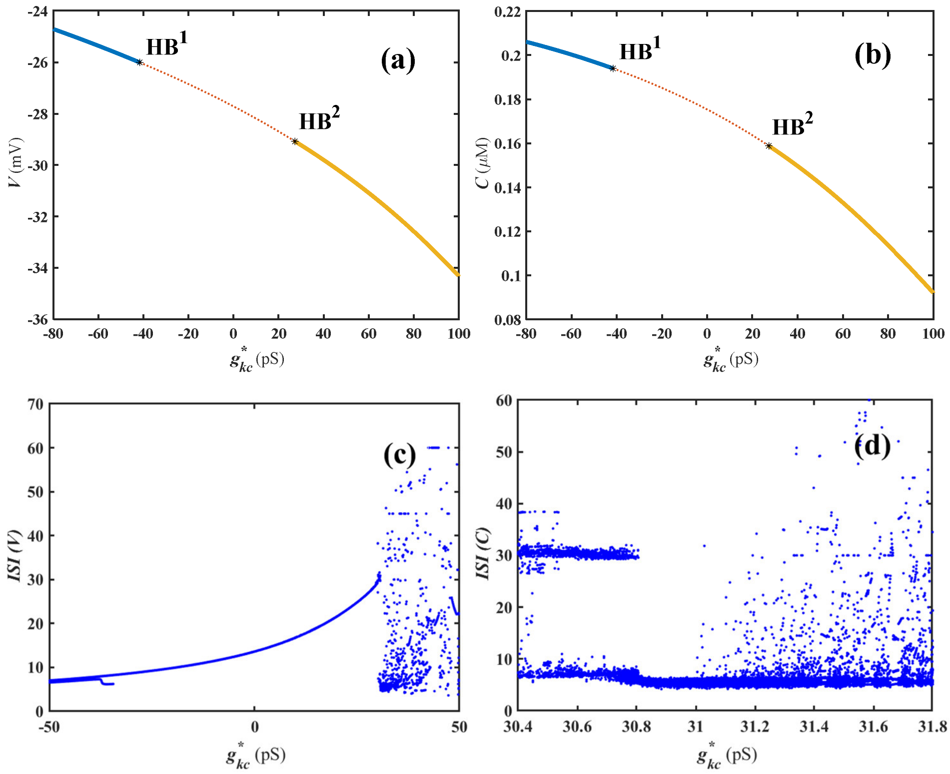

Figure 1. (Color online) (a) Bifurcation diagram of system (2) in the (g^*_{kc}, V) plane. (b) Bifurcation diagram of system (2) in the (g^*_{kc}, C) plane. HB^1 and HB^2 represent two Hopf bifurcation points. (c) The interspike interval (ISI) bifurcation of equilibrium with V and g^*_{kc}. (d) Enlargement of the interspike interval (ISI) bifurcation of equilibrium with C and g^*_{kc} in the selected range.

Because of the fluctuation in the parameter g^*_{kc}, the two Hopf bifurcation points are plainly visible. It can be seen that g^*_{kc} has a stable equilibrium between g^*_{kc} = -80 pS and -41.647 pS, as well as between g^*_{kc} = 27.25 pS and 100 pS. There are two unstable equilibria in the range of g^*_{kc} = -41.647 pS to 27.25 pS. Firing activities can be obtained from the ISI bifurcation with variation of the parameter g^*_{kc}. As g^*_{kc} is increased approximately to 30 pS, simple firing activities occur (Figure 1(c)). Then, in Figure 1(d), a partially enlarged picture of the ISI bifurcation in the (g^*_{kc}, C) plane is shown. As g^*_{kc} is increased to 31 pS, bursts are observed.

The corresponding time series of system (2) are presented in Figure 2. Figure 2(a1),(b1),(c1),(d1) shows the time evolution of parameter g^*_{kc} with different values. Figure 2(a2),(b2),(c2),(d2) represents distinct state trajectories in the three-dimensional phase space under different g^*_{kc} values.

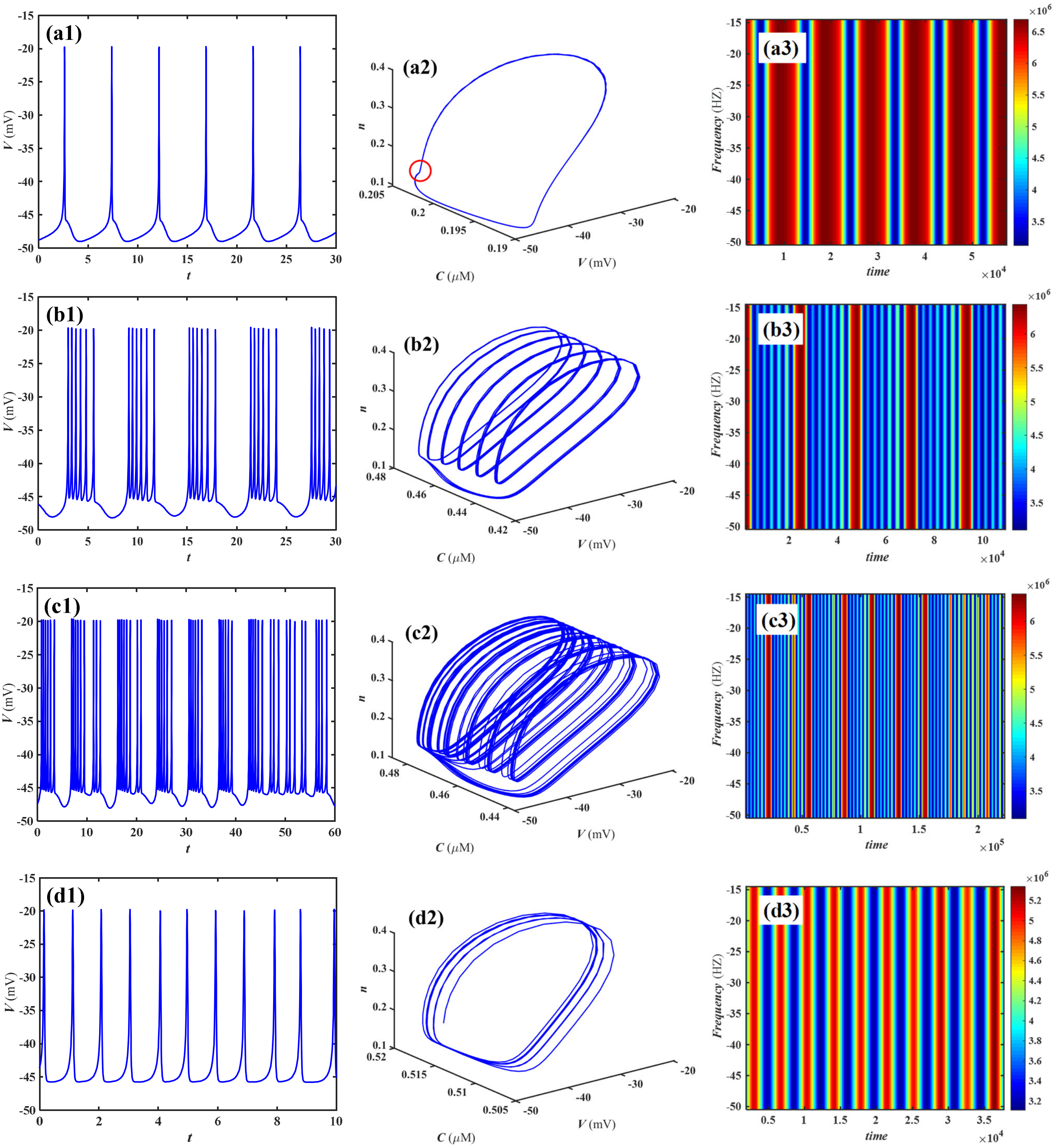

Figure 2. (Color online) Evolution of the membrane potential (V) in pyramidal neuron emerged in different parts of the curves relative to HB^1 and HB^2 points in Figure 1(a). (a1),(b1),(c1),(d1) The left column represents the temporal evolution of neuronal membrane potential (V) under different parameters g^*_{kc}. (a2),(b2),(c2),(d2) The image in the middle column denotes the corresponding V-C-n phase portrait. (a3),(b3),(c3),(d3) The image of the right column is recorded as the spectrum corresponding to Figure (a1)–(d1). (a) $g^*_{kc} = 21$ pS, (b) $g^*_{kc} = 11$ pS, (c) $g^*_{kc} = 10.9$ pS, (d) $g^*_{kc} = 10.4$ pS.

Figure 2 depicts the time-varying membrane voltage for various values of the parameter g^*_{kc}. On the left, the time evolution of V is compared with g^*_{kc}. The state trajectories in the 3D phase portrait V-

C-n space are shown in the middle panels, and the right panels are the time-frequency of parameter g^*_{kc}. For instance, there is a single peak in the oscillation when $g^*_{kc} = 21$ pS in Figure 2(a1). The one-to-one correspondence of the three-dimensional phase space is visualized in Figure 2(a2). Moreover, Figure 2(a3) shows a temporal-spectral pattern with the parameter $g^*_{kc} = 21$ pS. When the value of the bifurcation parameter g^*_{kc} drops, the total number of peak counts and magnitudes begins to increase. Similarly, six peaks were produced when $g^*_{kc} = 11$ pS, as shown in Figure 2(b1). Then, in Figure 2(c2), chaos appears. Furthermore, the number of peak counts in Figure 2(d1) tends to oscillate in a periodic fashion. Figure 2(a3),(b3),(c3),(d3) illustrates the frequency spectrogram of the temporal evolution pattern, making the change observation more apparent.

The membrane voltage of neurons exhibits spontaneous oscillations in Figure 2(a1). The temporal evolution Figure 2(a1), which corresponds to the 3D phase Figure 2(a2), appears as an inflection point, denoted by a red hollow circle. Figure 2(b1) displays a multi-peak oscillation phenomenon as the parameter g^*_{kc} lowers continually, in contrast to the single-peak oscillation phenomenon in Figure 2(a1). Among these, Figure 2(a1),(b1),(d1) represents a regular burst of membrane potential (V). Figure 2(c1) depicts chaos. In the third experimental situation, the evolution diagram of time shows significant irregularity, that is, the irregular spike sequence of spontaneous oscillations of membrane voltage (V). These phenomena are plentiful and warrant further investigation.

4. Conclusions

Mathematical modeling and numerical simulation are two effective methods to help us understand the internal workings of the neuronal system. We investigated the properties of primitive hippocampal neurons in the Chay model using the bifurcation parameter g^*_{kc}. We analyzed the theoretical stability of equilibrium and bifurcation and explored the variations in the conductance of the Ca^{2+}-sensitive K^+ channel. As the parameter g^*_{kc} varies, two supercritical Hopf critical nodes were found.

The Chay model exhibited a bi-stability phenomenon, namely the coexistence of chaotic attractors and stationary point attractors. This phenomenon was numerically revealed through time evolution, local bifurcation, phase planes and spectrum diagrams. Numerical calculations of Hopf bifurcations confirmed the theoretical analysis. It is concluded that the conductance of Ca^{2+}-sensitive K^+ channels leads to the emergence of complex neuronal bursting. Thus, some dynamic behaviors of system (1) are schematically presented. Measurements corroborated the numerical results, displaying dynamic behaviors. Validation of theoretical results was achieved through the use of numerical methods, which were employed after conducting a thorough theoretical analysis. Other complex dynamical behaviors of the presented Chay model should be further studied. We aim to conduct more comprehensive research on the relationship between the synchronization of oscillatory patterns and bifurcation in our upcoming investigations.

Use of AI tools declaration

The authors declare they have not used Artificial Intelligence (AI) tools in the creation of this article.

Acknowledgments

This work was supported by the National Natural Science Foundation of China (No. 12062004), the Natural Science Foundation of Guangxi Minzu University (No. 2022KJQD01), the Guangxi Natural Science Foundation (2020GXNSFAA297240), Guangxi Science and Technology Program (Grant No. AD23023001) and Xiangsi Lake Young Scholars Innovation Team of Guangxi Minzu University (No. 2021RSCXSHQN05).

Conflict of interest

The authors declare there is no conflict of interest.

References

1. K. Koyama, H. Ando, K. Fujiwara, Functional improvement in β cell models of type 2 diabetes using on-demand feedback control, *AIP Adv.*, **13** (2023), 045317. https://doi.org/10.1063/5.0124625
2. Z. Yang, Q. Lu, L. Li, The genesis of period-adding bursting without bursting-chaos in the Chay model, *Chaos, Solitons Fractals*, **27** (2006), 689–697. https://doi.org/10.1016/j.chaos.2005.04.038
3. Z. Yang, Q. Lu, H. Gu, W. Ren, Integer multiple spiking in the stochastic Chay model and its dynamical generation mechanism, *Phys. Lett. A*, **299** (2002), 499–506. https://doi.org/10.1016/S0375-9601(02)00746-6
4. M. Gu, Y. Zhu, X. Yin, D. M. Zhang, Small-conductance Ca^{2+}-activated K^+ channels: insights into their roles in cardiovascular disease, *Exp. Mol. Med.*, **50** (2018), 1–7. https://doi.org/10.1038/s12276-018-0043-z
5. X. Chen, Y. Feng, R. J. Quinn, D. L. Pountney, D. R. Richardson, G. D. Mellick, et al., Potassium channels in parkinson's disease: potential roles in its pathogenesis and innovative molecular targets for treatment, *Pharm. Rev.*, **75** (2023), 758–788. https://doi.org/10.1124/pharmrev.122.000743
6. J. P. Adelman, J. Maylie, P. Sah, Small-conductance Ca^{2+}-activated K^+ channels: form and function, *Annu. Rev. Physiol.*, **74** (2012), 245–269. https://doi.org/10.1146/annurev-physiol-020911-153336
7. M. Al-Khannaq, J. Lytton, Regulation of K^+-Dependent Na^+/Ca^{2+}-Exchangers (NCKX), *Int. J. Mol. Sci.*, **24** (2023), 598. https://doi.org/10.3390/ijms24010598
8. S. Song, L. Luo, B. Sun, D. Sun, Roles of glial ion transporters in brain diseases, *Glia*, **68** (2020), 472–494. https://doi.org/10.1002/glia.23699
9. Y. Li, R. Wang, T. Zhang, Nonlinear computational models of dynamical coding patterns in depression and normal rats: from electrophysiology to energy consumption, *Nonlinear Dyn.*, **107** (2022), 3847–3862. https://doi.org/10.1007/s11071-021-07079-7
10. L. Li, Z. Zhao, White-noise-induced double coherence resonances in reduced Hodgkin-Huxley neuron model near subcritical Hopf bifurcation, *Phys. Rev. E: Stat. Nonlinear Soft Matter Phys.*, **105** (2022), 034408. https://doi.org/10.1103/PhysRevE.105.034408
11. P. Crotty, K. Segall, D. Schult, Biologically realistic behaviors from a superconducting neuron model, *IEEE Trans. Appl. Supercond.*, **33** (2023), 1–6. https://doi.org/10.1109/TASC.2023.3242901

12. L. Blomer, On the voltage gated ion channels involved in action potential generation and back propagation in layer 5 pyramidal neurons, 2022. Available from: https://theses.hal.science/tel-04077615/file/BLOMER_2022_archivage.pdf.
13. M. V. Roshchin, V. N. Ierusalimsky, P. M. Balaban, E. S. Nikitin, Ca^{2+}-activated KCa3.1 potassium channels contribute to the slow afterhyperpolarization in L5 neocortical pyramidal neurons, *Sci. Rep.*, **10** (2020), 14484. https://doi.org/10.1038/s41598-020-71415-x
14. R. Orfali, N. Albanyan, Ca^{2+}-Sensitive potassium channels, *Molecules*, **28** (2023), 885. https://doi.org/10.3390/molecules28020885
15. L. Duan, Q. Lu, Q. Wang, Two-parameter bifurcation analysis of firing activities in the Chay neuronal model, *Neurocomputing*, **72** (2008), 341–351. https://doi.org/10.1016/j.neucom.2008.01.019
16. L. Duan, Q. Lu, Codimension-two bifurcation analysis on firing activities in Chay neuron model, *Chaos, Solitons Fractals*, **30** (2006), 1172–1179. https://doi.org/10.1016/j.chaos.2005.08.179
17. L. Duan, Q. Lu, Bursting oscillations near codimension-two bifurcations in the Chay Neuron model, *Int. J. Nonlinear Sci. Numer. Simul.*, **7** (2006), 59–64. https://doi.org/10.1515/IJNSNS.2006.7.1.59
18. Q. Xu, X. Tan, D. Zhu, H. Bao, Y. Hu, B. Bao, Bifurcations to bursting and spiking in the Chay neuron and their validation in a digital circuit, *Chaos, Solitons Fractals*, **141** (2020), 110353. https://doi.org/10.1016/j.chaos.2020.110353
19. Q. Xu, X. Tan, D. Zhu, M. Chen, J. Zhou, H. Wu, Synchronous behavior for memristive synapse-connected Chay twin-neuron network and hardware implementation, *Math. Probl. Eng.*, **2020** (2020), 8218740. https://doi.org/10.1155/2020/8218740
20. L. Lu, M. Yi, Z. Gao, Y. Wu, X. Zhao, Critical state of energy-efficient firing patterns with different bursting kinetics in temperature-sensitive Chay neuron, *Nonlinear Dyn.*, **111** (2023), 16557–16567. https://doi.org/10.1007/s11071-023-08700-7
21. L. L. Lu, M. Yi, X. Q. Liu, Energy-efficient firing modes of chay neuron model in different bursting kinetics, *Sci. China Technol. Sci.*, **65** (2022), 1661–1674. https://doi.org/10.1007/s11431-021-2066-7
22. F. Zhu, R. Wang, K. Aihara, X. Pan, Energy-efficient firing patterns with sparse bursts in the Chay neuron model, *Nonlinear Dyn.*, **100** (2020), 2657–2672. https://doi.org/10.1007/s11071-020-05593-8
23. T. R. Chay, Chaos in a three-variable model of an excitable cell, *Physica D*, **16** (1985), 233–242. https://doi.org/10.1016/0167-2789(85)90060-0